

### Radiation from creeping waves on micrometer-size perfectly conducting fibers

Y. T. Chu, R. D. Birkhoff, and H. H. Hubbell, Jr.\*

Health and Safety Research Division, Oak Ridge National Laboratory, Oak Ridge, Tennessee 37830, and Physics Department, The University of Tennessee, Knoxville, Tennessee 37916

(Received 25 February 1981)

The asymptotic solution of light scattering from a perfectly conducting circular cylinder is derived using the Watson transformation method first applied by Franz. It is clearly demonstrated that the scattered pattern is a superposition of a reflected wave and radiation from two creeping waves propagating around the cylinder in opposite directions. An He-Ne laser was used as a light source with  $\vec{H}$  field parallel to the axis of an aluminum-coated quartz fiber at normal incidence. The positions of intensity maxima and minima of the scattered light predicted by the Franz theory were not fully in agreement with experiment. We found it necessary to consider the phase change of the reflected wave in order to obtain satisfactory agreement.

#### INTRODUCTION

The scattering of electromagnetic waves at normal incidence by an infinitely long, homogeneous, circular cylinder was first treated by Lord Rayleigh.<sup>1</sup> This was later extended to oblique incidence by Wait.<sup>2</sup> The numerical calculation of the solution can be carried out for radii not larger than a few times the wavelength. A recent publication<sup>3</sup> describes this method of calculation and gives some experimental results. However, problems arise for larger radii. Since the solutions contain harmonic series with argument  $ka$  (where  $k$  is the wave number outside the cylinder, and the  $a$  radius of the cylinder), for large  $ka$  the series in the solution converges slowly. The work of Lundberg<sup>4</sup> gives a detailed description of the light scattering from conducting cylinders for  $ka$  greater than 50 by using the Fraunhofer diffraction equation and the approximate scattering function. The more accurate asymptotic solution for large  $ka$  can be obtained by two different methods. One is by means of an integral equation of the surface currents or fields at the surface currents or fields at the surface. This has been used by Fock<sup>5</sup> and later by Franz and Deppermann.<sup>6</sup> The second method is the use of the Watson transformation as proposed by Franz.<sup>7</sup> The asymptotic solution has the advantages of simplifying the calculation and of giving a physical model of the exact solution. It clearly demonstrates that the field outside a perfectly conducting cylinder is a superposition of an incident wave, a reflected wave, and two creeping waves. The creeping waves are injected at the shadow boundaries and creep into the shadow region, continuously spraying electromagnetic radiation forward tangentially away from the surface as they travel around the cylinder. A strong creeping wave is obtained for the incident wave with  $\vec{H}$  parallel to the axis of the cylinder, whereas

a relatively weak creeping wave is obtained for the incident wave with  $\vec{E}$  parallel to the axis of the cylinder. The creeping wave is of major importance in explaining the scattering problem in the shadow region as well as in the lighted region.

#### THEORY

We consider a perfectly conducting circular cylinder of radius  $a$ , having its axis along the  $z$  axis of a Cartesian coordinate system. Let a plane wave be incident along the  $x$  axis (see Fig. 1). If the incident magnetic field is in the  $z$  direction,

$$\vec{H}_z^i = e^{-ikx} \hat{z}, \tag{1}$$

and the total magnetic field at a point  $(\rho, \phi)$ , in a cylindrical coordinate system, outside the cylinder is<sup>8</sup>

$$\begin{aligned} H_z &= H_z^i + H_z^s \\ &= e^{-ik\rho \cos \phi} - \sum_{m=-\infty}^{\infty} (-i)^m e^{im\phi} \frac{J'_m(ka)}{H_m^{(1)'}(ka)} H_m^{(1)}(k\rho) \\ &= \sum_{m=-\infty}^{\infty} (-i)^m e^{im\phi} \left( J_m(k\rho) - \frac{J'_m(ka)}{H_m^{(1)'}(ka)} H_m^{(1)}(k\rho) \right), \end{aligned} \tag{2}$$

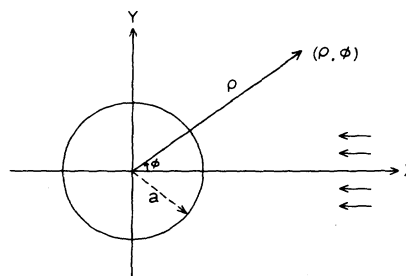


FIG. 1. Light scattering from a circular cylinder at normal incidence.

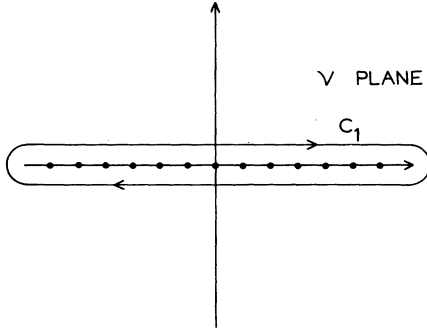


FIG. 2. The contour  $c_1$  encircling the real axis in the  $\nu$  plane, the dots representing integers.

where  $H_x^i$  is the incident wave,  $H_x^s$  is the scattered wave,  $J_m$  is a Bessel function of order  $m$ ,  $H_m^{(1)}$  is a Hankel function of the first kind and order  $m$ , and the prime denotes differentiation with respect to the argument. A time dependence  $e^{-i\omega t}$  is assumed.

The series given in Eq. (2) converges slowly for large values of  $ka$ . In order to find the asymptotic solution for large values of  $ka$ , Franz<sup>7</sup> used the classical method of the Watson transformation to convert the series into a contour integral

$$H_x = \frac{i}{2} \int_{c_1} \frac{e^{i\nu(\phi-\pi)}}{\sin \nu\pi} B_\nu d\nu, \quad (3)$$

where we have put

$$B_\nu = \frac{1}{2} \frac{e^{-i\nu\pi/2}}{H_\nu^{(1)'}(ka)} [H_\nu^{(1)'}(ka)H_\nu^{(2)}(k\rho) - H_\nu^{(2)'}(ka)H_\nu^{(1)}(k\rho)]. \quad (4)$$

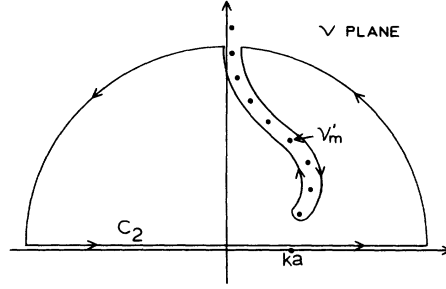


FIG. 3. The deformed integration path. The dots are zeros of  $H_{\nu'_m}^{(1)'} = 0$ .

The contour  $c_1$  is a closed contour encircling the entire real axis in the  $\nu$  plane as shown in Fig. 2.

With the relations

$$H_{-\nu}^{(1)}(x) = e^{i\nu\pi} H_\nu^{(1)}(x)$$

and

$$H_{-\nu}^{(2)}(x) = e^{-i\nu\pi} H_\nu^{(2)}(x),$$

we have  $B_{-\nu} = B_\nu$  and

$$H_x = i \int_{c_2} \frac{\cos \nu(\phi - \pi)}{\sin \nu\pi} B_\nu d\nu, \quad (5)$$

where the path of integration  $c_2$  is slightly above the real axis in the  $\nu$  plane. Now close the contour  $c_2$  with a large semicircle in the upper half plane as shown in Fig. 3.

It can be shown that the contribution from the semicircular arc vanishes as the arc radius approaches infinity; then the integral can be evaluated by computing the residues at the zeros  $\nu'_m$  of  $H_\nu^{(1)'}(ka)$ . We obtain

$$H_x = \pi \sum_{m=1}^{\infty} \frac{H_{\nu'_m}^{(2)'}(ka)}{\left(\frac{\partial}{\partial \nu} H_\nu^{(1)'}(ka)\right)\Big|_{\nu=\nu'_m}} \frac{e^{-i\nu'_m\pi/2} \cos \nu'_m(\phi - \pi)}{\sin \nu'_m\pi} H_{\nu'_m}^{(1)}(k\rho), \quad (6)$$

where  $\nu'_m$  has the form  $\nu'_m = ka - q'_m e^{i\pi/3} (ka/2)^{1/3}$ . The numerical values of  $-q'_m$  and associated values of the Airy functions  $\text{Ai}(q'_m)$  are given in Table I.<sup>9</sup> We note that the imaginary of  $\nu'_m$  is positive.

The Airy function representations of  $H_{\nu'_m}^{(1)'}(ka)$  and  $[\partial H_\nu^{(1)'}(ka)/\partial \nu]\Big|_{\nu=\nu'_m}$  are given as

$$H_{\nu'_m}^{(2)'}(ka) \approx \frac{e^{-i\pi/6}}{\pi \text{Ai}(q'_m)} \left(\frac{2}{ka}\right)^{2/3} \quad (7)$$

and

$$\left(\frac{\partial}{\partial \nu} H_\nu^{(1)'}(ka)\right)\Big|_{\nu=\nu'_m} \approx \frac{4q'_m}{ka} \text{Ai}(q'_m). \quad (8)$$

The asymptotic expression of  $H_{\nu'_m}^{(1)}(k\rho)$  for large  $k\rho$  is

$$\begin{aligned} H_{\nu'_m}^{(1)}(k\rho) &\approx \left(\frac{2}{\pi(k^2\rho^2 - \nu'^2)^{1/2}}\right)^{1/2} \exp\left\{i\left[(k^2\rho^2 - \nu'^2)^{1/2} - \nu'_m \cos^{-1}\left(\frac{\nu'_m}{k\rho}\right) - \pi/4\right]\right\} \\ &\approx \left(\frac{2}{\pi k(\rho^2 - a^2)^{1/2}}\right)^{1/2} \exp\left\{i\left[k(\rho^2 - a^2)^{1/2} - \nu'_m \cos^{-1}\left(\frac{a}{\rho}\right) - \frac{\pi}{4}\right]\right\}. \end{aligned} \quad (9)$$

The asymptotic solution in the *shadow region* can be obtained by substituting Eqs. (7), (8), and (9) into Eq. (6) and using the following relations

$$\frac{e^{-i\nu'_m\pi/2}\cos[\nu'_m(\phi-\pi)]}{\sin\nu'_m\pi} = -i \sum_{n=0}^{\infty} \{\exp[i\nu'_m(2n\pi+\phi-\pi/2)] + \exp[i\nu'_m(2n\pi+3\pi/2-\phi)]\}$$

and

$$\nu'_m = ka - q'_m e^{i\pi/3} \left(\frac{ka}{2}\right)^{1/3}.$$

We have the total field

$$H_z = H_z^{cw1} + H_z^{cw2}, \quad (10)$$

where

$$H_z^{cw1} = \frac{(ka)^{1/3} \exp\{i[k(\rho^2 - a^2)^{1/2} + \pi/12]\}}{[2k(\rho^2 - a^2)^{1/2}]^{1/2}} \sum_{m=1}^{\infty} \sum_{n=0}^{\infty} D_m \exp[-E_m(ka)^{1/3} \phi_{n1}] \exp\{i[ka + F_m(ka)^{1/3}] \phi_{n1}\}, \quad (11)$$

and

$$H_z^{cw2} = \frac{(ka)^{1/3} \exp\{i[k(\rho^2 - a^2)^{1/2} + \pi/12]\}}{[2k(\rho^2 - a^2)^{1/2}]^{1/2}} \sum_{m=1}^{\infty} \sum_{n=0}^{\infty} D_m \exp[-E_m(ka)^{1/3} \phi_{n2}] \exp\{i[ka + F_m(ka)^{1/3}] \phi_{n2}\}, \quad (12)$$

where we have put

$$\phi_{n1} = 2n\pi + \left(\phi - \frac{\pi}{2} - \cos^{-1} \frac{a}{\rho}\right), \quad (13a)$$

$$\phi_{n2} = 2n\pi + \left(\frac{3\pi}{2} - \phi - \cos^{-1} \frac{a}{\rho}\right), \quad (13b)$$

$$D_m = 2^{-1/3} \pi^{-1/2} \{(-q'_m)[\text{Ai}(q'_m)]^2\}^{-1}, \quad (13c)$$

$$E_m = (-q'_m)2^{-1/3} \sin\pi/3, \quad (13d)$$

$$F_m = (-q'_m)2^{-1/3} \cos\pi/3. \quad (13e)$$

The numerical values of  $D_m$ ,  $E_m$ , and  $F_m$  are given in Table II.  $H_z^{cw1}$  and  $H_z^{cw2}$  may be interpreted as follows. The angular dependence phases in Eqs. (11) and (12) are proportional to the angles  $\phi_{n1}$  and  $\phi_{n2}$ , respectively. These angles are mea-

sured from the shadow boundaries and correspond to the paths of rays traveling along the surface of the cylinder. For this reason, they are called creeping waves. The geometrical representation of creeping waves  $H_z^{cw1}$  and  $H_z^{cw2}$  is given in Fig. 4. The summation over  $m$  goes from 1 to infinity; therefore creeping waves  $H_z^{cw1}$  and  $H_z^{cw2}$  have an infinite number of modes, and the velocities of the creeping waves for different modes on the surface of the cylinder are  $c/[1 + F_m(ka)^{-2/3}]$ , where  $c$  is the velocity of light in the vacuum. The summation over  $n$  indicates the number of turns of the creeping wave traveling around the cylinder surface. The exponents of the damping factors are determined by the imaginary part of  $\nu'_m$  which is proportional to  $-q'_m$ . The value of  $-q'_m$  is larger for larger  $m$  (see Table I); there-

TABLE I. Zeros and associated values of the Airy functions.

$m$	$-q'_m$	$\text{Ai}(q'_m)$
1	1.0188	+0.5357
2	3.2482	-0.4190
3	4.8201	+0.3804
4	6.1633	-0.3579
5	7.3722	+0.3423
6	8.4885	-0.3305
7	9.5354	+0.3210
8	10.5277	-0.3132
9	11.4751	+0.3065
10	12.3848	-0.3007

TABLE II. The numerical values of  $D_m$ ,  $E_m$ , and  $F_m$  for the first ten modes of the creeping waves.

$m$	$D_m$	$E_m$	$F_m$
1	1.5316	0.7003	0.4043
2	0.7853	2.2327	1.2890
3	0.6420	3.3132	1.9129
4	0.5672	4.2364	2.4459
5	0.5184	5.0674	2.9257
6	0.4830	5.8347	3.3687
7	0.4558	6.5543	3.7841
8	0.4336	7.2364	4.1779
9	0.4154	7.8876	4.5539
10	0.3999	8.5129	4.9149

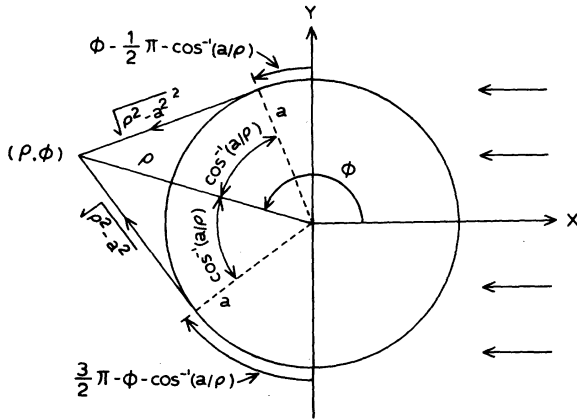


FIG. 4. The geometrical representation of the creeping waves in the shadow region.

fore, the first mode of the creeping wave gives the largest contribution to the field.

In the *lighted region*, the derivation is slightly different. Substituting the relation

$$H_z^{cw1'} = \frac{(ka)^{1/3} \exp\{i[k(\rho^2 - a^2)^{1/2} + \pi/12]\}}{[2k(\rho^2 - a^2)^{1/2}]^{1/2}} \sum_{m=1}^{\infty} \sum_{n=0}^{\infty} D_m \exp[-E_m(ka)^{1/3} \phi'_{n1}] \exp\{i[ka + F_m(ka)^{1/3}] \phi'_{n1}\} \quad (14b)$$

and

$$H_z^{cw2'} = \frac{(ka)^{1/3} \exp\{i[k(\rho^2 - a^2)^{1/2} + \pi/12]\}}{[2k(\rho^2 - a^2)^{1/2}]^{1/2}} \sum_{m=1}^{\infty} \sum_{n=0}^{\infty} D_m \exp[-E_m(ka)^{1/3} \phi'_{n2}] \exp\{i[ka + F_m(ka)^{1/3}] \phi'_{n2}\}, \quad (14c)$$

where we have put

$$\phi'_{n1} = 2n\pi + \left(\frac{3\pi}{2} + \phi - \cos^{-1} \frac{a}{\rho}\right), \quad (15a)$$

$$\phi'_{n2} = 2n\pi + \left(\frac{3\pi}{2} - \phi - \cos^{-1} \frac{a}{\rho}\right). \quad (15b)$$

If the observation point is far away from the cylinder, then  $\phi'_{n1}$  and  $\phi'_{n2}$  in Eqs. (15a) and (15b) can be replaced as

$$\phi'_{n1} = 2n\pi + (\pi + \phi), \quad (16a)$$

$$\phi'_{n2} = 2n\pi + (\pi - \phi). \quad (16b)$$

The numerical values of  $D_m$ ,  $E_m$ , and  $F_m$  are given in Table II. Equations (14b) and (14c) represent two creeping waves in the lighted region. The geometrical representation of creeping waves  $H_z^{cw1'}$  and  $H_z^{cw2'}$  in the lighted region is given in Fig. 5.

The second integral  $I_2$  can be evaluated by the method of stationary phase.<sup>10</sup> If we deform the path of integration to pass through the stationary points  $k\rho[\sin(\phi)]$  and  $ka[\sin(\phi/2)]$  (see Fig. 6), we can obtain

$$\cos\nu(\phi - \pi) = e^{i\nu\pi} \cos\nu\phi - ie^{i\nu\phi} \sin\nu\pi$$

into Eq. (5), we have

$$H_z = I_1 + I_2,$$

where

$$I_1 = i \int_{c_2} \frac{e^{i\nu\pi} \cos\nu\phi}{\sin\nu\pi} B_\nu d\nu$$

and

$$I_2 = \int_{c_2} e^{i\nu\phi} B_\nu d\nu.$$

The first integral  $I_1$  can be evaluated by closing the contour  $c_2$  in the upper half of the  $\nu$  plane and integrating about the residues at zeros of  $H_{\nu_m}^{(1)'}(ka) = 0$ . We obtain

$$I_1 = H_z^{cw1'} + H_z^{cw2'}, \quad (14a)$$

where

$$I_2 = I_{2a} + I_{2b}, \quad (17a)$$

with

$$I_{2a} = e^{-ik\rho \cos\phi}, \quad (17b)$$

and

$$I_{2b} = \left(\frac{a \cos(\phi/2)}{2\rho}\right)^{1/2} \exp\{ik(\rho - 2a \cos(\phi/2))\}. \quad (17c)$$

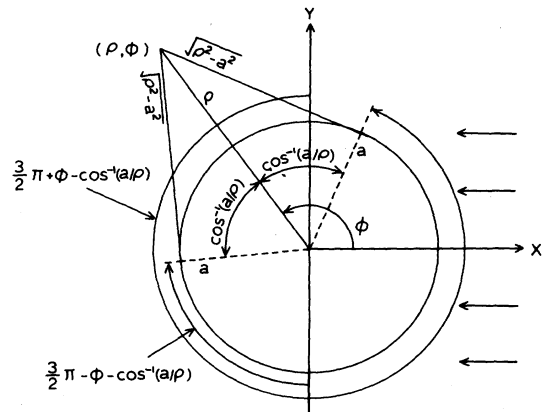


FIG. 5. The geometrical representation of the creeping waves in the lighted region.

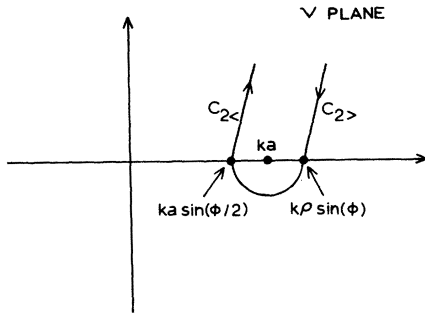


FIG. 6. The deformed integration path passes the stationary points for evaluation in geometrical optics field.

The quantities  $I_{2a}$  and  $I_{2b}$  represent the incident wave and reflected wave, respectively. If we neglect the contribution of the creeping waves in the lighted region, then  $I_{2a}$  and  $I_{2b}$  are just the leading terms of the asymptotic solution which is deduced by the methods of Luneberg and Kline.<sup>11</sup> The total field  $H_z$  outside the cylinder in the lighted region is the superposition of the incident wave, the reflected wave, and two creeping waves. That is,

$$H_z = H_z^i + H_z^s, \quad (18a)$$

$$H_z^i = I_{2a}, \quad (18b)$$

$$H_z^s = I_{2b} + I_1. \quad (18c)$$

## RESULTS

The quartz fibers were prepared by the method described by Neher.<sup>12,3</sup> They were mounted between straight pins glued 7 cm apart on an aluminum support which was painted with black paint to prevent reflection from the support. The support was covered temporarily with a piece of aluminum foil. The entire assembly was then positioned in a bell-jar evaporator above the evaporating source, and the fiber and mount were rotated about the fiber axis while metal was evaporated onto the fiber. The order of 500 Å of aluminum was deposited, which represents an effectively infinitely thick layer at the He-Ne laser wavelength of 6328 Å. The aluminum foil was then removed from the support. The aluminized-quartz fiber was set on a three dimensionally adjustable arm, which is mounted in a 3700 series ORTEC scattering chamber. A 1P28 photomultiplier detector was housed in a box with a slit of width about 0.25 cm. In order to prevent non-uniform response of the photocathode, a piece of Scotch tape was used as a diffuser on the slit. The radii of the fibers had been checked by a

scanning electron microscope and compared with a standard aperture. We adjusted the radii slightly from the values measured by the scanning electron microscope (less than 3%) to get the best fit with the experimental data. The fibers designated A1-1 and A1-2 have adjusted radii of 1.481 and 1.715 μm, respectively. The distance from the fiber to the photomultiplier is about 20 cm. The plane wave of the He-Ne laser is incident perpendicular to the axis of the fiber with  $\vec{H}_i$  parallel to the axis of the fiber and produces strong creeping waves.

The values of  $ka$  for the fibers A1-1 and A1-2 at wavelength 6328 Å are 14.7 and 17.0, respectively. The distance from the fiber to the photomultiplier is relatively large compared to the radii of the fibers; thus the field at the photomultiplier represents the far zone field. Moreover, the width of the slit is also large compared to the radii of the fibers; thus the equations for the lighted region can be used for theoretical calculations. In the far zone, we have  $H_z = E_\phi$ . The angular distribution of the scattered energy is the time-average Poynting vector  $\vec{S}$  in the radial direction; thus we have

$$\vec{S} = \frac{c}{8\pi} |H_z|^2.$$

If  $I_0$  denotes the intensity of the incident wave and  $I$  the intensity of wave scattered in the direction  $\phi$  at a large distance  $\rho$  from the cylinder, then the ratio of  $I$  to  $I_0$  is

$$\frac{I}{I_0} = \frac{|H_z^s|^2}{|H_z^i|^2}. \quad (19)$$

The theoretical calculations can be obtained by substituting Eqs. (18), (17), (16), and (14) into the above equation. If we choose only the first mode of the creeping waves (i.e.,  $m=0$ ), the theoretical results and experimental data for the fibers A1-1 and A1-2 are given in Figs. 7(a) and 7(b). We can see that the positions of intensity maxima and minima predicted by the theory are not in good agreement with experiments, especially near the forward scattering region ( $\phi \sim \pi$ ). This may be attributed to the series given in Eq. (14c) yielding a poor convergence for  $\phi \sim \pi$  and  $n=0$ . If  $\phi \sim \pi$  and  $n=0$ , Eq. (16b) gives  $\phi'_{n2} \sim 0$ . The exponent of the damping factor, which is  $-E_m(ka)^{1/3} \phi'_{n2}$ , in Eq. (14c) is small for  $\phi'_{n2} \sim 0$ ; thus the series has a poor convergence when  $\phi$  approaches  $\pi$ . It is necessary to choose more terms (i.e., more modes of the creeping waves) in Eq. (14c) to make the series converge. If we choose 10 modes of the creeping waves (i.e., the summation over  $m$  from 1-10), the series converges approximately in the regions ( $0^\circ < \phi < 170^\circ$ )

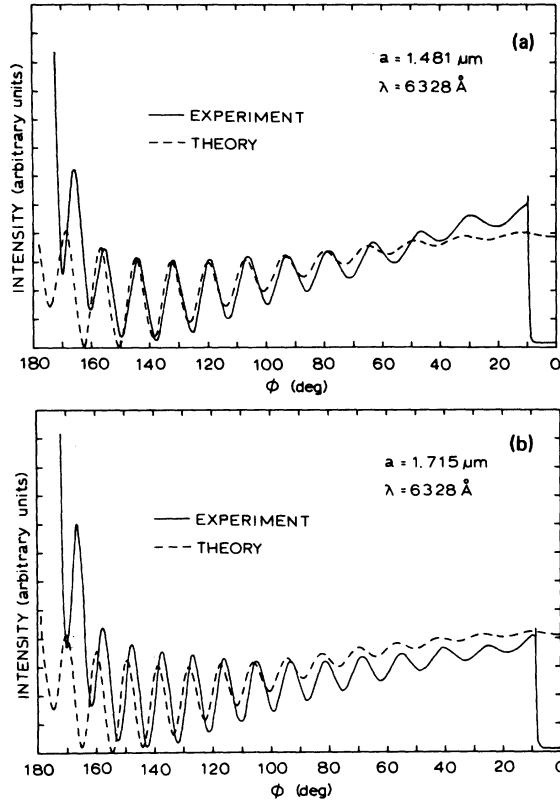


FIG. 7. (a) Scattering from fiber Al-1. The first mode of the creeping waves is used in the Franz theory. (b) Scattering from fiber Al-2. The first mode of the creeping waves is used in the Franz theory.

and ( $0^\circ < \phi < 174^\circ$ ) for fibers Al-1 and Al-2, respectively. The theoretical results and experimental data for the fibers Al-1 and Al-2 are given in Figs. 8(a) and 8(b). These figures show that even though we took 10 modes of the creeping waves for the calculations of Eq. (14c), it still did not improve the agreement with experiment much even in the convergent regions.

One consideration which was omitted in the calculation was the phase change of the reflected wave from the conducting cylinder. This will be considered next.

#### The phase change of reflected wave

The theory derived above is based on the assumptions that the value of  $ka$  is large and the cylinder is a perfect conductor. Since aluminum is a good conductor, we assume that the creeping waves are damped by spraying electromagnetic radiation and by Joule losses. The path lengths of the creeping waves traveling on the surface of the cylinder are so short that we can ignore the effect of Joule losses.<sup>13</sup> The phase change of the reflected wave has to be examined in more

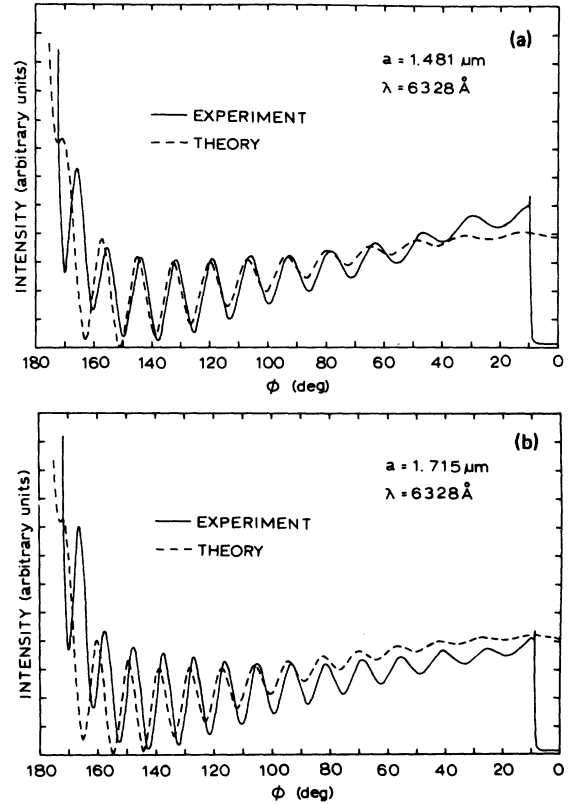


FIG. 8. (a) Scattering from fiber Al-1. The first ten modes of the creeping waves are used in the Franz theory. (b) Scattering from fiber Al-2. The first ten modes of the creeping waves are used in the Franz theory.

detail. Since the value of  $ka$  is large and the radius of the cylinder is larger than the wavelength, we can assume that the surface is locally flat for the reflected wave. If the conductor is a non-magnetic material, the phase change and the amplitude of the reflected wave for different polarizations of incident plane wave are given in the following<sup>14</sup>:

$$\vec{E}_1^r = \rho_\perp e^{i\Delta_\perp} \vec{E}_1^i, \quad (20a)$$

$$\vec{H}_1^r = \rho_\parallel e^{i\Delta_\parallel} \vec{H}_1^i, \quad (20b)$$

where  $E_1^i$  is the incident wave with  $E$  field normal to the plane of incidence,  $E_1^r$  is the reflected wave with  $E$  field normal to the plane of incidence,  $H_1^i$  is the incident wave with  $H$  field normal to the plane of incidence,  $H_1^r$  is the reflected wave with  $H$  field normal to the plane of incidence,

$$\rho_\perp^2 = \frac{(A - \cos\theta)^2 + B^2}{(A + \cos\theta)^2 + B^2},$$

$$\tan \Delta_\perp = \frac{-2B \cos\theta}{\cos^2\theta - A^2 - B^2},$$

$$\rho_{\parallel}^2 = \frac{(A - \cos\theta)^2 + B^2}{(A + \cos\theta)^2 + B^2} \frac{(A - \sin\theta \tan\theta)^2 + B^2}{(A + \sin\theta \tan\theta)^2 + B^2},$$

$$\tan\Delta_{\parallel} = \frac{-2B(A^2 + B^2 - \sin^2\theta)\cos\theta}{A^2 + B^2 - (N^2 + K^2)\cos^2\theta},$$

$$A^2 = \frac{1}{2} \{ [(N^2 - K^2 - \sin^2\theta)^2 + 4N^2K^2]^{1/2} + (N^2 - K^2 - \sin^2\theta) \},$$

$$B^2 = \frac{1}{2} \{ [(N^2 - K^2 - \sin^2\theta)^2 + 4N^2K^2]^{1/2} - (N^2 - K^2 - \sin^2\theta) \},$$

and the angle of incidence  $\theta$  is equal to the angle of reflection  $\phi/2$ .

Substituting  $N=1.40$  and  $K=7.45$  for aluminum (at  $6328 \text{ \AA}$ ) (Ref. 15) in the above equations gives the calculated phase change shown in Fig. 9. In our experiments, the incident plane wave has an  $H$  field parallel to the axis of the cylindrical fiber; thus the plane of incidence is normal to the fiber axis and the phase change of the reflected wave is  $\Delta_{\parallel}$ . The angle of incidence is near  $\pi/2$  in the forward scattering region. Figure 9 shows that the phase change  $\Delta_{\parallel}$  changes significantly for the angle of incidence near  $\pi/2$ .

Now we consider a simple model in which the intensity of scattered wave is produced by the interference of three types of waves scattered from a cylinder: the ordinary wave reflected with phase change and two creeping waves propagated around the surface of the cylinder in opposite directions and radiating as they travel. The reflected wave can be obtained from Eqs. (20b) and (17c),

$$H_{\parallel}^r = \left( \frac{a \cos(\phi/2)}{2\rho} \right)^{1/2} \rho_{\parallel} \exp(i\{\Delta_{\parallel} + k[\rho - 2a \cos(\phi/2)]\}).$$

The scattered wave can be written as

$$H_{\parallel}^s = H_{\parallel}^r + I_1.$$

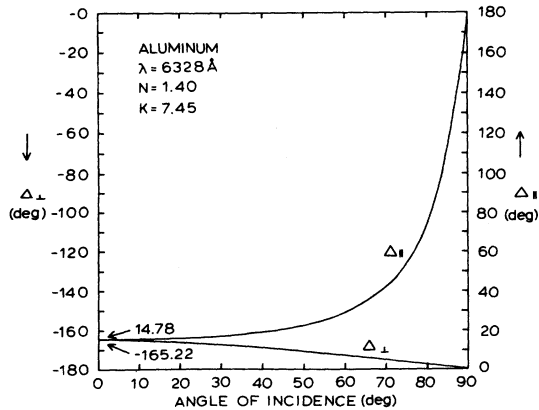


FIG. 9. The phase changes of the reflected wave for different orientations of polarizations of incident plane waves.

The theoretical calculations of Eq. (19) for fibers Al-1 and Al-2 are given in Figs. 10(a) and 10(b), which include only one mode for the creeping waves, and in Figs. 11(a) and 11(b), which include the first ten modes for the creeping waves. These figures show that the positions of intensity maxima and minima agree well with the experiments, if we consider the phase change of the reflected wave.

## CONCLUSION

We have calculated from the creeping wave theory of Franz the angular distribution of parallel light scattered by a micrometer-size fiber. Experiments were conducted on aluminized-quartz fibers with a He-Ne laser and photomultiplier detector for comparison with the theory. Agreement was only approximate due to the neglecting in the theory of the phase change of the reflected light which forms an interference pattern with the light spray from the creeping waves of Franz. Introduction of the phase change of reflected light

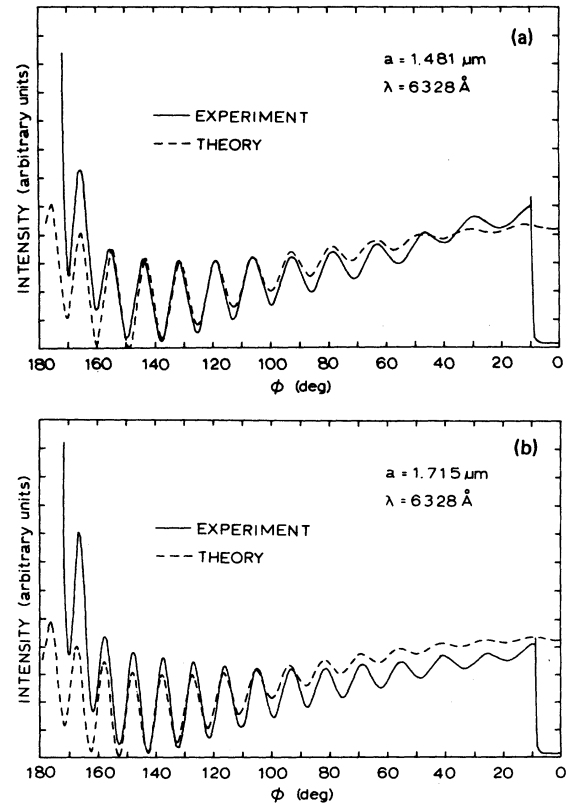


FIG. 10. (a) Scattering from fiber Al-1. The first mode of the creeping waves is used, and the phase change of the reflected wave is included. (b) Scattering from fiber Al-2. The first mode of the creeping waves is used, and the phase change of the reflected wave is included.

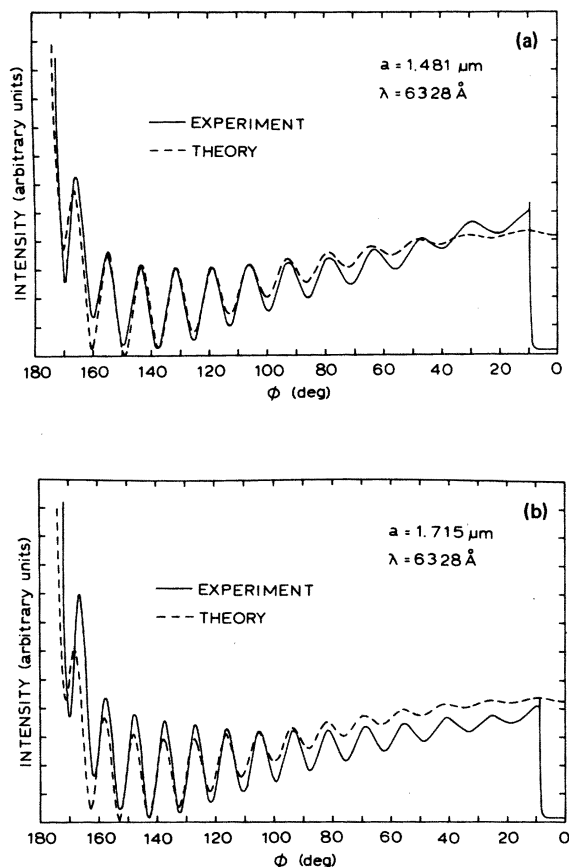


FIG. 11. (a) Scattering from fiber Al-1. The first ten modes of the creeping waves are used, and the phase change of the reflected wave is included. (b) Scattering from fiber Al-2. The first ten modes of the creeping waves are used and the phase change of the reflected wave is included.

improves the agreement of the positions of intensity maxima and minima substantially. Better agreement of the magnitude of the intensity of scattered light is achieved if more modes are included in the creeping waves.

The pattern of the scattered light from a circular cylinder is a complete ring around the cylinder, and the intensity of the scattered light is angularly symmetric with respect to  $\phi = 0$  and  $\phi = \pi$ . The theoretical calculation of Eqs. (14) and (16) for the scattered light is only applicable in the range of  $\phi$  from 0 to  $\pi$  or from 0 to  $-\pi$ . If  $|\phi|$  exceeds  $\pi$ , then either  $\phi'_{n1}$  or  $\phi'_{n2}$  in Eqs. (14) and (16) is negative; and this makes the exponent of the damping factor in Eq. (14) positive so that the series diverges.

The creeping waves are damped very rapidly by spraying electromagnetic radiation, and thus they travel only a very short distance and make only a few revolutions on the surface of the cylinder. Thus the summation over  $n$  in Eq. (14) can be taken for only a few terms without loss of accuracy. It is interesting to note that the calculations of the positions of intensity maxima and minima for the scattered light are not very sensitive to the changing of the optical constants  $N$  and  $K$ .

#### ACKNOWLEDGMENTS

This research was sponsored by the Office of Health and Environmental Research, U. S. Department of Energy, under Contract No. W-7405-eng-26 with the Union Carbide Corporation, and in part, by the U. S. Army Research Office under Interagency Agreement DOE Contract No. 40-1094-80.

\*Science Applications, Inc., Oak Ridge, Tennessee, and La Jolla, California.

<sup>1</sup>Lord Rayleigh, *Philos. Mag.* **12**, 81 (1881).

<sup>2</sup>J. R. Wait, *Can. J. Phys.* **33**, 189 (1955).

<sup>3</sup>R. D. Birkhoff, J. C. Ashley, H. H. Hubbell, Jr., and L. C. Emerson, *J. Opt. Soc. Am.* **67**, 564 (1977).

<sup>4</sup>J. L. Lundberg, *J. Colloid Interface Sci.* **29**, 565 (1969).

<sup>5</sup>V. A. Fock, *J. Phys. (Moscow)* **10**, 130 (1946).

<sup>6</sup>W. Franz and K. Deppermann, *Ann. Phys. (Leipzig)* **10**, 361 (1952).

<sup>7</sup>W. Franz, *Naturforscher* **9**, 705 (1954).

<sup>8</sup>M. Kerker, *The Scattering of Light and Other Electromagnetic Radiation* (Academic, New York, 1969), Chap. 6, pp. 255-263.

<sup>9</sup>M. Abramowitz and I. A. Stegun, *Handbook of Mathematical Functions* (Dover, New York, 1965), p. 478.

<sup>10</sup>H. Jeffreys and B. S. Jeffreys, *Methods of Mathematical Physics* (Cambridge University, London, 1950), pp. 503-507.

<sup>11</sup>J. B. Keller, R. M. Lewis, and B. D. Seckler, *Commun. Pure Appl. Math.* **9**, 207 (1956).

<sup>12</sup>V. Neher, *Procedures in Experimental Physics*, edited by John Strong (Prentice-Hall, New York, 1943), Chap. 5, pp. 205-207.

<sup>13</sup>H. C. van de Hulst, *Light Scattering by Small Particles* (Wiley, New York, 1957), Chap. 17, p. 369.

<sup>14</sup>J. A. Stratton, *Electromagnetic Theory* (McGraw-Hill, New York, 1941), Chap. 9, pp. 505-506.

<sup>15</sup>H. -J. Hagemann, W. Gudat, and C. Kunz, Report No. DESY. SR-74/7 (available from Deutsches Elektronen Synchrotron DESY, 2 Hamburg 52, West Germany).